Scripta Materialia 130 (2017) 78–82

Contents lists available at ScienceDirect

Scripta Materialia

journal homepage: www.elsevier.com/locate/scriptamat

Regular Article

Temperature dependent fracture initiation in microscale silicon

Eric D. Hintsala [a,b,*], Sanjit Bhowmick [a], Xie Yueyue [c], Roberto Ballarini [c], S. A. Syed Asif [a], William W. Gerberich [b]

[a] Hysitron Inc., Minneapolis, MN, USA
[b] University of Minnesota, Department of Chemical Engineering and Materials Science, Minneapolis, MN, USA
[c] University of Houston, Department of Civil Engineering, Houston, TX, USA

ARTICLE INFO

Article history:
Received 8 November 2016
Received in revised form 14 November 2016
Accepted 14 November 2016
Available online 24 November 2016

Keywords:
Silicon
Fracture
Brittle-to-ductile transition
Nanomechanical testing
Electron microscopy

ABSTRACT

We present novel in-situ scanning electron microscope experiments exploring the fracture of silicon as a function of temperature at the microscale, from room temperature to 600 °C. Clear post mortem TEM observations of dislocation activity at and above 450 °C suggest that back stresses from crack-tip dislocation emission raise the applied stress intensity at initiation, as part of a brittle to ductile transition starting at 300 °C. This is in agreement with other microscale measurements; however, these experiments are particularly noteworthy in their ability to directly observe crack advance and perform post-mortem analysis to investigate dislocation activity.

© 2016 Acta Materialia Inc. Published by Elsevier Ltd. All rights reserved.

1. Introduction

Silicon remains one of the most important technological materials in use today, especially for interconnected electronics at the micro and nanoscale [1,2]. King et al.'s research update [1] proposed that combined material, metrology and modeling approaches will be essential to 3D transistor and interconnect success in approaching the 5 nm scale. While this can be easily accomplished using multi-scale modeling, understanding of the thermal, flow stress, fracture mechanics and scaling behavior is severely lacking at the sub-micron scale. New metrologies must be developed to provide verifiable property relations for multi-scale simulations [1,2]. Silicon represents a model material for understanding brittle-to-ductile transitions (BDT), possessing a rapid transition occurring in the vicinity of 600–650 °C, identified long ago [3]. However, this transition is affected by variables [4] including size [5], strain rate [6,7], stress state [6,7] and impurity content [8]. Under some of these variable ranges, silicon can behave in a highly ductile manner through dislocation emission. For instance, previous work on compression of Si nanocubes (20–50 nm in size) [9,10] showed large plastic strains over 50% with no indication of fracture. Eventually, activation volumes and critical stresses, which can be determined from targeted experiments, will be needed to establish relationships between deformation mechanisms and these variables. For micro- and nanoscale mechanical measurements, various methodologies and equipment have been rapidly developed over the past decade [9–23]. Of these, use of focused ion beam (FIB) – fabricated specimens which are loaded by a nanoindenter system are popular [15–23], as the necessary equipment can be utilized to create multiple testing configurations from bulk or thin film materials. The present study demonstrates the ability to study fracture in microscale silicon as a function of temperature using such tools. This is accomplished using 1 μm thick, doubly-clamped, pre-notched bending beams with in-situ SEM at temperatures up to 600 °C with a fixed strain rate and impurity condition, representing only a small piece of the DBT variable spectrum for silicon.

2. Experimental

The base material utilized is a silicon wedge (~30 μm tall with a 1 μm width at the narrowest top portion) substrate, which is fabricated using KOH etching from a ⟨001⟩ silicon wafer, p-type doped with a final resistivity of 0.001–0.005 Ω-cm, corresponding to 1×10^{19}–1×10^{20} cm^{-3} boron doping. This material was ideal for focused ion beam (FIB) machining due to its well-defined crystallographic orientation and small material removal requirements. Using an FEI Versa FIB/SEM, bending specimens were prepared using Ga^{+} ions at 30 keV accelerating voltage, with progressively decreasing beam current from 3 nA down to 10 pA as the cuts became finer. Final shaping cuts were performed at a 2° tilt into the specimen to reduce FIB taper. The FIB machining process was a slightly modified version of that described in Appendix A of [22]. For the in situ testing configuration, shown in Fig. 1a, FIB machining from the top exposes {110} surfaces, whose zone axis was parallel to the electron beam, while the indenter loaded the specimen parallel to a {100} zone axis. The targeted geometry was a 10 μm span, 2 μm width, and 1 μm thickness. The specimens were pre-notched using a FIB line cutting mode with 10 pA current and 2° tilt. The notch was targeted to be 1/3 of

* Corresponding author at: Hysitron Inc., Minneapolis, MN, USA.
E-mail address: ehintsala@hysitron.com (E.D. Hintsala).

http://dx.doi.org/10.1016/j.scriptamat.2016.11.016
1359-6462/© 2016 Acta Materialia Inc. Published by Elsevier Ltd. All rights reserved.

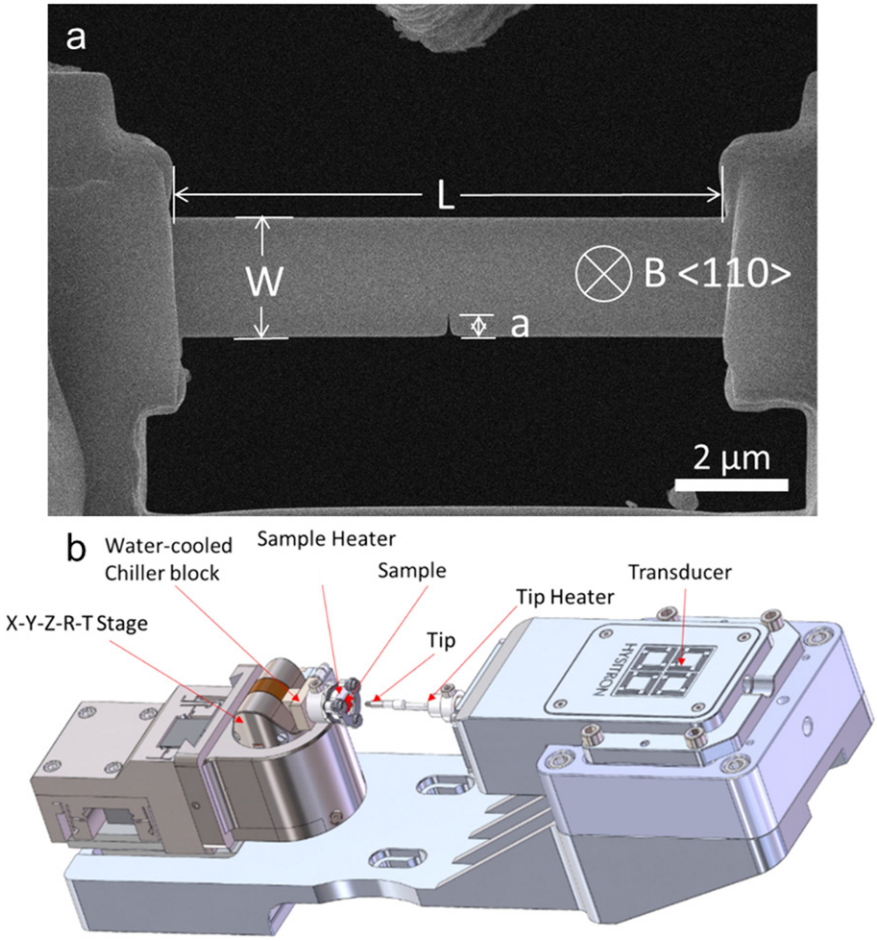

Fig. 1. a) SEM micrograph of as fabricated pre-notched microscale Si bending beam, with important quantities marked: L (length), W (width), B (thickness), a (notch length). Note this is an earlier specimen with a/W = 0.2 compared to a/W = 0.33 for the majority of the work which produced no significant difference in results. b) Schematic of Hysitron PI-87 SEM indenter system with integrated tip and sample heaters.

the beam width, or 0.667 μm and resulted in notches with a radius of curvature of 15–35 nm.

Testing was performed with a Hysitron PI-88 in-situ SEM PicoIndenter inside an FEI Versa dual beam FIB/SEM operating at 20 keV. Specimens were loaded using a wedge geometry probe with a nominally flat contact surface 1 μm in width and 14 μm long. Loading was performed in displacement control at 10 nm/s, corresponding to a maximum bending strain rate of 0.0006 s^{-1}. Drift correction was performed utilizing the in-situ videos to adjust the measured displacement to the actual beam deflection. A novel Hysitron-designed heater system which integrated with the PI 88 PicoIndenter, shown in Fig. 1b, was utilized to control the temperature. This system utilizes separate resistive sample and probe heaters, which are independently feedback-controlled to improve tip-sample equilibrium and reduce drift. The screw down clamping mechanism allowed the specimen to freely expand perpendicular to the indentation axis, thus eliminating thermal stresses. All samples were annealed at 600 °C for 1 h prior to testing and each test temperature setpoint was allowed to settle for 30 min. Additionally, beneficial effects in terms of recrystallizing the surface damage from the FIB process may have occurred as recently demonstrated for Si [23], but this was not verified for these specimens.

The tested specimens were also thinned for post-mortem TEM via FIB from the top to ~200 nm thickness utilizing a 100 pA beam current. The sample was then mounted to a Hysitron PI-95 PicoIndenter for imaging in an FEI F30 TEM operating at 300 keV. Bright field images were taken aligned near the ⟨110⟩ zone axis with 1 s exposure time.

3. Results & discussion

Bending experiments were carried out on 28 separate microbeams at temperatures of 25, 150, 300, 450 and 600 °C, with 5–6 tests per temperature. In Fig. 2a, example load-displacement curves are shown for each temperature. For room temperature up to 450 °C, the load-displacement response appeared to be classically brittle with a load drop associated with crack nucleation and extension followed by further linear loading. At the highest test temperature of 600 °C, the load-displacement curve instead flattens upon crack initiation which is indicative of plasticity. This is also apparent when examining post-mortem SEM images as shown in the Fig. 2a insets, where residual bending can be observed in the 600 °C specimen. After some initial elastic deflection, all tested specimens nucleated a center crack extending from the notch accompanied by a load drop. This initiation point was chosen for further analysis, plotted for all specimens in Fig. 2b, as later load drops were complicated by secondary cracking near the clamping constraints in accordance with FEM simulations and experiments done by Jaya et al. [20, 21]. By comparison, observation of crack initiation from the notch associated with the first load drop was clear, as shown in the inset for Fig. 2b. An interesting trend in the crack initiation load can be observed where initially the load decreases from room temperature to 150 °C, then increases up to 600 °C.

To examine the fracture load trend in greater detail, a finite element method (FEM) analysis was carried out. The FEM analysis was accomplished using an average of the dimensions of the as-FIBed bending

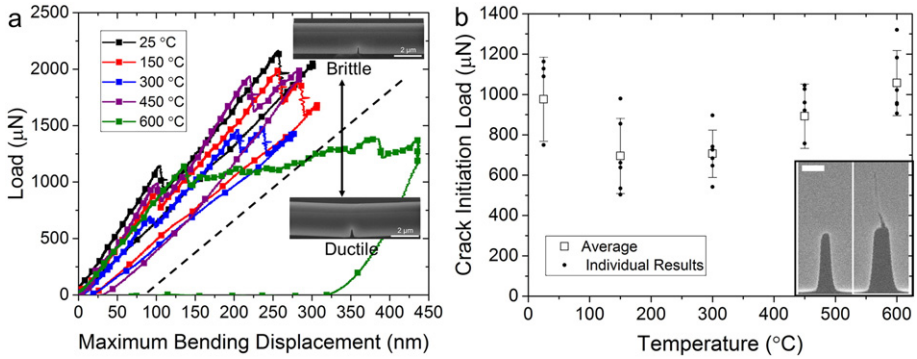

Fig. 2. a) Load displacement curves for a representative bending beam experiments, with postmortem SEM insets showing the change from brittle to ductile behavior at 600 °C and b) summary of loads for fracture initiation. Inset: in-situ SEM of crack initiation resulted in a rapid crack advance, scale bar 250 nm.

beams (as measured by SEM), with isotropically averaged values of Poisson's ratio and elastic moduli. A resulting applied K_I, normalized by the applied load, was calculated for several crack lengths along the bending beam, which is shown in Fig. 3a. The K_{II} curve was calculated to be less than 0.1% of the K_I magnitude in all cases and is thus not considered further. It can be observed that the applied stress intensity reaches its maximum at 667 nm, the targeted FIB notch length, which is in agreement with [20,21]. This effectively decreases the applied mode I stress intensity at the crack or notch the further it has extended across the beam. This configuration is then self-arresting, making imaging and post-mortem analysis more feasible.

Perhaps the most obvious complication of these experiments is the radius of curvature of the notch, which varied from 15 to 35 nm for these experiments due to operating of the FIB near its resolution limits. One can apply a first order correction factor, K′/K, where K′ is the increased stress intensity due to the radius of curvature and K is the actual stress intensity, based upon the plastic zone size as suggested by [18]

$$\frac{K'}{K} = \sqrt{1 + \frac{\rho}{2d_0}}; \quad \text{where } d_0 = \frac{2}{\pi}\frac{K_{Ic}^2}{\sigma_y^2} \tag{1}$$

with K_{Ic} the fracture toughness and σ_y the yield strength as applied to a notch with radius ρ. In order to utilize this correction factor, the required material inputs are the yield strength, and the fracture toughness. Utilizing strength measurements from 1 μm micropillars produced from the same wedge substrate (3 pillars at 300 °C and 3 pillars at 600 °C), which produced comparable results to 880 nm micropillars compressed by Rabier [17], a linear strength vs. temperature relationship of $\sigma_{ys}(GPa) = 10.624 - .01044(T(K))$ was used. For the fracture toughness input, the room temperature, bulk value of 0.7 MPa-m$^{1/2}$ was utilized. The resulting stress intensity determined from the curve in Fig. 3a is shown as a function of temperature in Fig. 3b as the uncorrected curve, which is compared against the notch sharpness corrected values. As the bending beam dimensions vary little between specimens, the fracture initiation load trend is reflected in the uncorrected values. For the sharpness corrected values, it can be observed that the initiation stress intensity factor was close to 0.7 MPa-m$^{1/2}$ from 25 to 300 °C before steadily increasing up to 600 °C, a more typical BDT transition with temperature which is a good match for results from silicon microcantilevers [19] and micropillars [16,17]. This analysis suggests that the change in plastic zone size as a function of temperature may have resulted in the fracture load trend from 25 to 300 °C. This furthermore suggests the increase in stress intensity from 300 to 600 °C may be based upon dislocation shielding since this is not a fracture toughness incorporating large plastic energy dissipation.

To explore the possibility of dislocation shielding at the higher temperatures further, post mortem TEM imaging of thinned bending beam specimens was performed. A set of example TEM micrographs are shown in Fig. 4(a–f), for specimens tested at different temperatures and bending displacements. It can be seen in Fig. 4a that at 300 °C no evidence of plasticity can be observed, which was similar to results at 25 and 150 °C test temperatures (not shown). Fig. 4b & c shows two examples at 450 °C test temperature, where in Fig. 4b (test terminated just after crack initiation), there is a small region of dark contrast underneath the FIB notch which may correlate to a plastic zone. The specimen in Fig. 4c underwent further bending and a small number of loops can be observed to expand from the crack arrest point. The results at 600 °C shown significantly increased dislocation activity in Fig. 4d & e, where a clear plastic zone is developed in Fig. 4d just after crack initiation. In Fig. 4e, with further bending, the entire area from the crack to the contact area is a plastic hinge consistent with the residual bending of the specimen; a full view of the specimen from Fig. 4e is shown in 4f to help contextualize the TEM images.

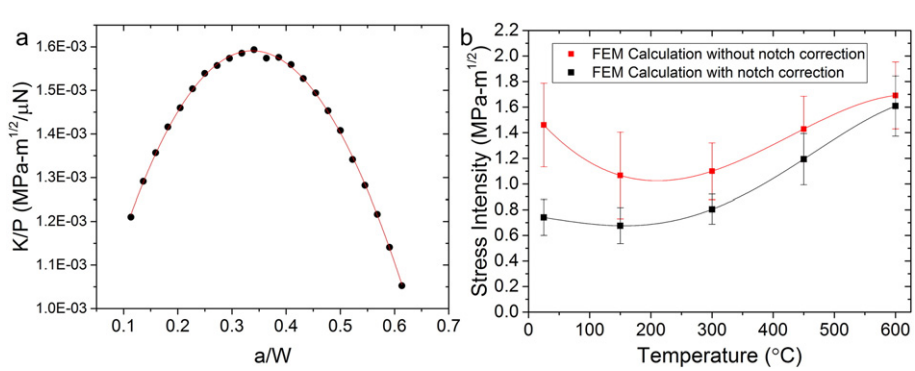

Fig. 3. a) FEM calculation of applied stress intensity at the crack tip normalized by load for Si bending beams vs. crack length normalized by beam width. A parabolic relationship is found (one point is noticeably off the curve due to some minor calculation error). b) Comparison of stress intensity for crack initiation from the FEM curve in (a) with and without notch sharpness correction.

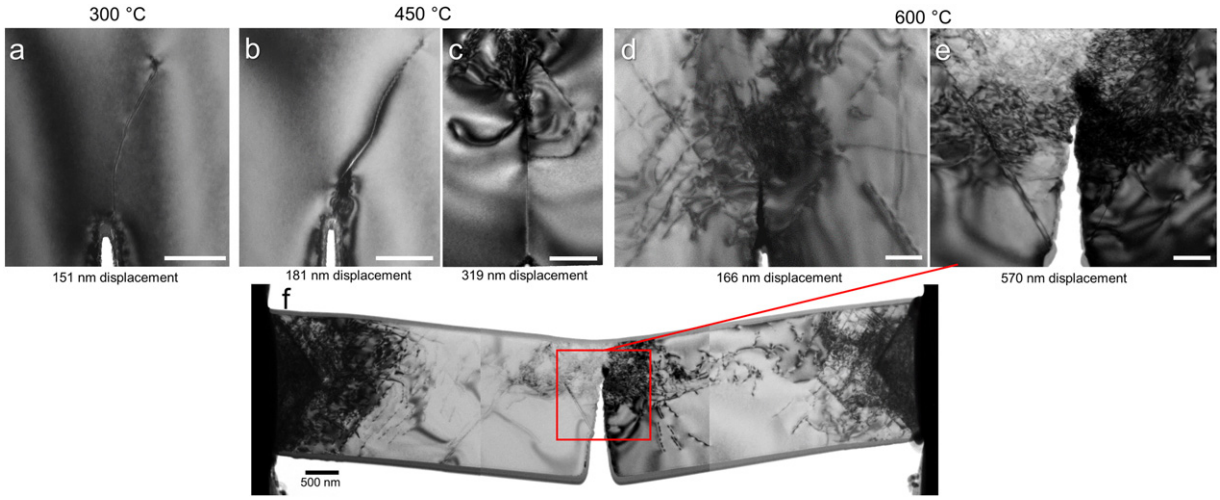

Fig. 4. Post-mortem TEM micrographs of the crack region of a microbeam deformed at: a) 300 °C, b) 450 °C and displacement just up to crack initiation, c) 450 °C and high displacement, d) 600 °C and displacement just up to crack initiation, and e) 600 °C and high displacement, scale bar 200 nm. In f), a stitched TEM image of the full bending beam from which (e) is taken. Note that the dense dislocation network at the ends of the bending beam formed after crack initiation.

The result in Fig. 4d is particularly interesting, as it has the clearest developed plastic zone. A promising capability of this experimental scheme is direct observation of dislocations surrounding a propagating crack for evaluating processes such as crack arrest and shielding. This will require more TEM imaging conditions and sectioning of other regions besides the central thickness for a complete picture, but this can be briefly demonstrated here. In Fig. 4d, a plastic zone diameter of $2r_p$ ~ 1000 nm was estimated. This can be utilized to obtain a first order plasticity estimate of the crack arrest toughness from

$$r_p = K_{Ia}^2/2\pi\sigma_{ys}^2 \tag{2}$$

where K_{Ia} is the crack arrest stress intensity, giving a value of 2.13 MPa-m$^{1/2}$, which is appropriately higher than the initiation intensity. Regarding the shielding, one can apply a back stress model to observed individual dislocations, such as the simplified 2D construction applied by Higashida et al. [24]. which gives a local shielding stress intensity, k_D, of

$$k_D = \sum_i \left\{ \frac{3\mu b_i}{(1-\nu)(2\pi r_i)^{1/2}} \cos(\Phi/2)\sin(\Phi) \right\} \tag{3}$$

where μb is the shear modulus times the Burgers vector, ν is Poisson's ratio, r_i is the dislocation distance of the i_{th} dislocation, and Φ is the angle between the slip plane and the crack tip. For Φ, an error estimate of $\pm$12% was determined using a mean value of 35° for the angle between the 100 crack propagation axis and a $\{\bar{1}11\}$ slip plane. If one assumes a partial dislocation burgers vector of 0.227 nm, a shear modulus of 68 GPa and the distance, r_i, for each dislocation in the apparent pile-up of 7 dislocations on the left hand side of the notch, a shielding stress intensity of 0.177 MPa-m$^{1/2}$ is determined. Since only one slip system was imaged realistically in 4f, due to a single g vector and a slight twist of the bending beam along the crack axis, clearly many shielding dislocations are missing. For these specimens, of the 12 available slip systems, 6 are capable of producing shielding of the crack tip resulting in a scaling up of the shielding estimate to 1.05 MPa-m$^{1/2}$. If this value is subtracted from the linear elastic FEM calculation of 1.65 MPa-m$^{1/2}$, a value of 0.6 MPa-m$^{1/2}$ is obtained, fairly close to the Griffith value based upon surface energy alone. All considered, the plastic zone estimate above giving a value of 2.13 MPa-m$^{1/2}$ might represent an upper bound giving rise to an estimate of 1.4 $\pm$ 0.7 MPa-m$^{1/2}$.

4. Conclusions

This study demonstrated the ability to utilize temperature control to explore fracture initiation in microscale bending specimens. Using FEM analysis and a notch sharpness correction factor, the loads for crack initiation were converted to stress intensities values which increased with test temperature according to a typical BDT curve. Here, a significant increase in stress intensity for crack initiation was observed which corresponded to nucleation of dislocations, confirmed by post-mortem thinning and TEM imaging. It appears reasonable to attribute the increased linear elastic stress intensity to dislocation shielding, though more careful future experiments are needed to confirm such a hypothesis. However, the results presented here are a promising starting point, from which more careful evaluation of notch effects, more detailed post-mortem TEM analysis of crack tip – dislocation interactions and exploration of more of the variable space controlling the DBT in silicon, such as strain rate or impurity content, could be pursued.

Acknowledgements

The authors would like to thank Ariel Leonard for her assistance with the high temperature fracture testing and Dr. Douglas D. Stauffer for his advice from Hysitron, Inc. Partial support came from the NSF MRSEC Program at the University of Minnesota, Award DMR-1420013. Parts of this work were carried out in the Characterization Facility, University of Minnesota, which receives partial support from NSF through the MRSEC program.

References

[1] S.W. King, H. Simka, D. Herr, H. Akinaya, M. Garner, Appl. Mater. 1 (2013) 040701.
[2] D. Josell, S.H. Brongersma, Z. Tokei, Annu. Rev. Mater. Sci. (2009) 231–254.
[3] C.S. John, Phil. Mag. 32 (1975) 1193–1212.
[4] E. Hintsala, C. Teresi, W.W. Gerberich, Met. Trans. A (2016) 1–6.
[5] F. Östlund, K. Rzepiejewska-Malyska, K. Leifer, L.M. Hale, Y. Tang, R. Ballarini, W.W. Gerberich, J. Michler, Adv. Funct. Mat. 19 (2009) 2439–2444.
[6] P.B. Hirsch, S.G. Roberts, Philos. T. R. Soc. A 355 (1997) 1991–2002.
[7] P.B. Hirsch, S.G. Roberts, Philos. Mag. A 64 (1991) 55–80.
[8] A. George, G. Champier, Phys. Stat. Sol. (a) 53 (1979) 529.
[9] A.J. Wagner, E.D. Hintsala, P. Kumar, W.W. Gerberich, K.A. Mkhoyan, Acta Mater. 100 (2015) 256–265.
[10] E.D. Hintsala, A.J. Wagner, W.W. Gerberich, K.A. Mkhoyan, Scr. Mater. 114 (2016) 51–55.
[11] J.D. Nowak, A.R. Beaber, O. Ugurlu, S.L. Girshick, W.W. Gerberich, Scr. Mater. 62 (2010) 819–822.
[12] R.H. Dauskardt, M. Lane, Q. Ma, N. Krishna, Eng. Fract. Mech. 61 (2007) 141–162.
[13] M.R. Begley, J.W. Hutchinson, J. Mech. Phys. Solids 46 (1998) 2049–2068.
[14] J.W. Hutchinson, Z. Suo, Adv. Appl. Mech. 29 (1992) 191.

[15] S. Korte, W.J. Clegg, Scr. Mater. 60 (2009) 807–810.
[16] S. Korte, J.S. Barnard, R.J. Stearn, W.J. Clegg, Int. J. Plast. 27 (2011) 1853–1866.
[17] J. Rabier, A. Montagne, J.M. Wheeler, J.L. Demenet, J. Michler, R. Ghisleni, Phys. Stat. Sol. (c) 10 (2013) 11–15.
[18] D.E.J. Armstrong, A.S.M.A. Haseeb, S.G. Roberts, A.J. Wilkinson, K. Bade, Thin Solid Films 520 (2012) 4369–4372.
[19] D.E. Armstrong, E. Tarleton, J. Mater. 67 (2015) 2914–2920.
[20] B.N. Jaya, V. Jayaram, S.K. Biswas, Philos. Mag. 92 (2012) 3326–3345.
[21] B.N. Jaya, V. Jayaram, Int. J. Fract. 188 (2014) 213–228.
[22] E. Hintsala, D. Kiener, J. Jackson, W.W. Gerberich, Exper. Mech. (2015) 1–10.
[23] Y.C. Wang, D.G. Xie, X.H. Ning, Z.W. Shan, Appl. Phys. Lett. 106 (2015) 081905.
[24] K.M. Higashida, M. Tanaka, A. Hartmaier, Y. Hoshino, Mater. Sci. Eng. A 483 (2008) 13–18.